

Exploring the Vulnerability of Deep Neural Networks: A Study of Parameter Corruption

Xu Sun^{1,*}, Zhiyuan Zhang^{1,*}, Xuancheng Ren¹, Ruixuan Luo¹, Liangyou Li²

¹ School of EECS, Peking University, ² Huawei Noah’s Ark Lab

{xusun, zzy1210, renxc, luoruixuan97}@pku.edu.cn, liliangyou@huawei.com

Abstract

We argue that the vulnerability of model parameters is of crucial value to the study of model robustness and generalization but little research has been devoted to understanding this matter. In this work, we propose an indicator to measure the robustness of neural network parameters by exploiting their vulnerability via parameter corruption. The proposed indicator describes the maximum loss variation in the non-trivial worst-case scenario under parameter corruption. For practical purposes, we give a gradient-based estimation, which is far more effective than random corruption trials that can hardly induce the worst accuracy degradation. Equipped with theoretical support and empirical validation, we are able to systematically investigate the robustness of different model parameters and reveal vulnerability of deep neural networks that has been rarely paid attention to before. Moreover, we can enhance the models accordingly with the proposed adversarial corruption-resistant training, which not only improves the parameter robustness but also translates into accuracy elevation.

1 Introduction

Despite the promising performance of Deep neural networks (DNNs), research has discovered that DNNs are vulnerable to adversarial examples, i.e., simple perturbations to input data can mislead models [14, 18, 21]. These findings concern vulnerability of DNNs against input data. However, the vulnerability of DNNs does not only exhibit in input data. As functions of both input data and model parameters, the parameters of neural networks are a source of vulnerability of equal importance. Especially, advances in hardware neural networks [25, 1, 30, 34, 2] also call for study in parameter vulnerability because of hardware deterioration and background noise, which can be seen as parameter corruption. More importantly, study on parameter vulnerability can deepen our understanding of various mechanisms in neural networks, inspiring innovation in architecture design and training paradigm.

To probe the vulnerability of neural network parameters and evaluate the *parameter robustness*, we propose an indicator that measures the maximum loss change caused by small perturbations on model parameters in the non-trivial worst-cased scenario. The perturbations can be seen as artificial parameter corruptions. We give an infinitesimal gradient-based estimation of the indicator that is efficient for practical

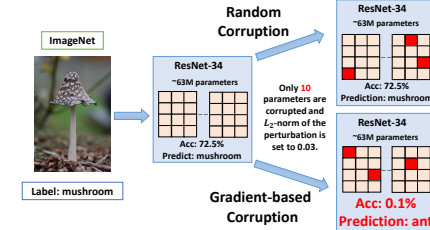


Figure 1: Parameter corruptions with ResNet-34 on ImageNet. It shows that deep neural networks are robust to random corruptions, but the accuracy can drop significantly in the worst case suggested by the gradient-based method. The accuracy is measured on the development set.

*Equally contributed.

purposes compared with random corruption trials, which can hardly induce optimal loss degradation. Our theoretical and empirical results both validate the effectiveness of the proposed gradient-based method. As shown in Figure 1, model parameters are generally resistant to random corruptions but the worst outlook can be quite bleak suggested by the gradient-based corruption result.

Intuitively, the indicator shows the maximum altitude ascent within a certain distance of the current parameter on the loss surface, as illustrated conceptually in Figure 2. The traditional learning algorithms focus on obtaining lower loss, which means generally the parameters at point B are preferred. However, the local geometry of the landscape also indicates the generalization performance of the learning algorithm [17, 4]. The parameters at point B demonstrate critical vulnerability to parameter corruptions, while the parameters at point A are a better choice since larger perturbations are required to render significant loss change. It is also observed in our experiments that the parameters at point A have better generalization performance as a result of corruption-resistance.

Equipped with the proposed indicator, we are able to systematically analyze the parameter robustness and probe the vulnerability of different components in a deep neural network via observing the accuracy degradation after applying corruptions to its parameters. Furthermore, the comparisons between the gradient-based and the random corruption for estimating the indicator suggest that the neighborhood of the learned parameters on the loss surface is generally flattish except for certain steep directions. If we can push the parameters away from the steep directions, the robustness of the parameters can be improved significantly. Therefore, we propose to conduct adversarial corruption-resistant training that incorporates virtual parameter corruptions to find parameters without steep directions in the neighborhood. Experimental results show that the proposed method not only improves the parameter robustness of deep neural networks but also elevates their accuracy in application tasks.

Our main contributions are as follows:

- To understand the parameter vulnerability of deep neural networks, which is fundamentally related to model robustness and generalization, we propose an indicator that measures the maximum loss change if small perturbations are applied on model parameters, i.e., parameter corruptions. The proposed gradient-based estimation is far more effective in exposing the parameter vulnerability than random corruption trials, validated by both theoretical and empirical results.
- The indicator is used to probe the vulnerability of different kinds of parameters with diverse structural characteristics in a trained neural network. Through systematic analyses of representative architecture across benchmark datasets, we summarize divergent vulnerability of neural network parameters, especially bringing attention to normalization layers.
- To improve the robustness of the models with respect to parameters, we propose to enhance the training of deep neural networks by taking the parameter vulnerability into account and introduce the adversarial corruption-resistant training that can improve the accuracy and the generalization performance of deep neural networks.

2 Parameter Corruption

In this section, we introduce the problem of parameter corruption and the proposed indicator. Then, we describe the Monte-Carlo estimation and the gradient-based estimation of the indicator backed with theoretical support.

Before delving into the specifics, we first introduce our notations. Let \mathcal{N} denote a neural network, $\mathbf{w} \in \mathbb{R}^k$ denote a k -dimensional subspace of its parameter space, and $\mathcal{L}(\mathbf{w}; \mathcal{D})$ denote the loss

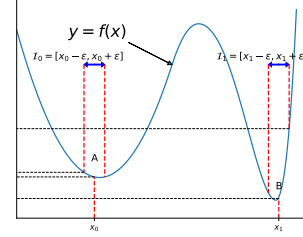


Figure 2: In this illustration of the loss function, traditional optimizer prefers B rather than A, because B has the lower loss. However, parameters at point B are more vulnerable to parameter corruption, as $\max_{x \in I_0} (f(x) - f(x_0)) < \max_{x \in I_1} (f(x) - f(x_1))$. Base on our experiments, we argue that parameters that are resistant to corruption, e.g., at point A, can embody potentially better robustness and generalization.

function of \mathcal{N} on the dataset \mathcal{D} , regarding to the specific parameter subspace \mathbf{w} . Taking a k -dimensional subspace allows a more general analysis on a specific group of parameters.

To expose the vulnerability of model parameters, we propose to adopt the approach of parameter corruption. To formally analyze its effect on neural networks and eliminate trivial corruption, we formulate the parameter corruption as a small perturbation $\mathbf{a} \in \mathbb{R}^k$ to the parameter vector \mathbf{w} . The corrupted parameter vector becomes $\mathbf{w} + \mathbf{a}$. The small perturbation requirement is realized as a constraint set of the parameter corruptions.

Definition 1 (Corruption Constraint). *The corruption constraint is specified by the set*

$$S = \{\mathbf{a} : \|\mathbf{a}\|_p = \epsilon \text{ and } \|\mathbf{a}\|_0 \leq n\}, \quad (1)$$

where $\|\cdot\|_0$ denotes the number of non-zero elements in a vector and $1 \leq n \leq k$ denotes the maximum number of corrupted parameters. ϵ is a small positive real number and $\|\cdot\|_p$ denotes the L_p -norm where $p \geq 1$ such that $\|\cdot\|_p$ is a valid distance in Euclidean geometry.

For example, $\mathbf{a} \in S = \{\mathbf{a} : \|\mathbf{a}\|_2 = \epsilon \text{ and } \|\mathbf{a}\|_0 \leq k\}$ specifies that the corruption should be on a k -dimensional sphere with a radius of ϵ and no limit on the number of corrupted parameters.

Suppose $\Delta\mathcal{L}(\mathbf{w}, \mathbf{a}; \mathcal{D}) = \mathcal{L}(\mathbf{w} + \mathbf{a}; \mathcal{D}) - \mathcal{L}(\mathbf{w}; \mathcal{D})$ denotes the loss change. To evaluate the effect of parameter corruption, it is most reasonable to consider the worst-case scenario and thus, we propose the indicator as the maximum loss change under the corruption constraints. The optimal parameter corruption is defined accordingly.

Definition 2 (Indicator and Optimal Parameter Corruption). *The indicator $\Delta_{\max}\mathcal{L}(\mathbf{w}, S, \mathcal{D})$ and the optimal parameter corruption \mathbf{a}^* are defined as:*

$$\Delta_{\max}\mathcal{L}(\mathbf{w}, S, \mathcal{D}) = \max_{\mathbf{a} \in S} \Delta\mathcal{L}(\mathbf{w}, \mathbf{a}, \mathcal{D}), \text{ and } \mathbf{a}^* = \arg \max_{\mathbf{a} \in S} \Delta\mathcal{L}(\mathbf{w}, \mathbf{a}, \mathcal{D}). \quad (2)$$

Let \mathbf{g} denote $\partial\mathcal{L}(\mathbf{w}; \mathcal{D})/\partial\mathbf{w}$ and H denote the Hessian matrix; suppose $\|\mathbf{g}\|_2 = G > 0$. Using the second-order Taylor expansion, we estimate the loss change and the indicator:

$$\Delta\mathcal{L}(\mathbf{w}, \mathbf{a}; \mathcal{D}) = \mathbf{a}^T \mathbf{g} + \frac{1}{2} \mathbf{a}^T H \mathbf{a} + o(\epsilon^2) = f(\mathbf{a}) + o(\epsilon). \quad (3)$$

Here, $f(\mathbf{a}) = \mathbf{a}^T \mathbf{g}$ is a first-order estimation of $\Delta\mathcal{L}(\mathbf{w}, \mathbf{a}; \mathcal{D})$ and meanwhile the inner product of the parameter corruption \mathbf{a} and the gradient \mathbf{g} , based on which we maximize the alternative inner product instead of initial loss function to estimate the indicator.

We provide and analyze two methods to understand the effect of parameter corruption, which estimate the value of the indicator based on constructive, artificial, theoretical parameter corruptions. Comparing the two methods, the random parameter corruption gives a Monte-Carlo estimation of the indicator and the gradient-based parameter corruption gives an infinitesimal estimation that can effectively capture the worst case. Please refer to Appendix for detailed proofs of propositions and theorems.

2.1 Random Corruption

We first analyze the random case. As we know, randomly sampling a perturbation vector \mathbf{a} does not necessarily conform to the constraint set S and it is complex to generate corruption uniformly distributed in S as the generation is determined by the shape of S and is not universal enough. In order to eliminate the problem, we define the random parameter corruptions used in this estimation as maximizing an alternative inner product $\mathbf{a}^T \mathbf{r}$ under the constraint, based on a random vector \mathbf{r} instead of the gradient \mathbf{g} to ensure the randomness.

Definition 3 (Random Parameter Corruption and Monte-Carlo Estimation). *Given a randomly sampled vector $\mathbf{r} \sim N(0, 1)$, a valid random corruption $\tilde{\mathbf{a}}$ for a Monte-Carlo estimation of the indicator in the constraint set S , which has a closed-form solution, is*

$$\tilde{\mathbf{a}} = \arg \max_{\mathbf{a} \in S} \mathbf{a}^T \mathbf{r} = \epsilon \left(\text{sgn}(\mathbf{h}) \odot \frac{|\mathbf{h}|^{\frac{1}{p-1}}}{\|\mathbf{h}\|^{\frac{1}{p-1}}}_p \right) \quad (4)$$

where $\mathbf{h} = \text{top}_n(\mathbf{r})$. The $\text{top}_n(\mathbf{v})$ function retains $\text{top-}n$ magnitude of all $|\mathbf{v}|$ dimensions and set other dimensions to 0, $\text{sgn}(\cdot)$ denotes the signum function, $|\cdot|$ denotes the point-wise absolute function, and $(\cdot)^\alpha$ denotes the point-wise α -power function. The loss change with the random corruption is a Monte-Carlo estimation of the indicator.

Algorithm 1 Random Corruption

Require: Parameter vector $\mathbf{w} \in \mathbb{R}^k$, set of corruption constraints S
1: Sample $\mathbf{r} \sim N(0, 1)$
2: Solve the random corruption $\tilde{\mathbf{a}}$ according to Eq.(4)
3: Update the parameter vector $\mathbf{w} \leftarrow \mathbf{w} + \tilde{\mathbf{a}}$

Algorithm 2 Gradient-Based Corruption

Require: Parameter vector $\mathbf{w} \in \mathbb{R}^k$, set of corruption constraints S , loss function \mathcal{L} and dataset \mathcal{D}
1: Obtain the gradient $\mathbf{g} \leftarrow \partial \mathcal{L}(\mathbf{w}; \mathcal{D}) / \partial \mathbf{w}$
2: Solve the corruption $\hat{\mathbf{a}}$ in Eq.(7) with S and \mathbf{g}
3: Update the parameter vector $\mathbf{w} \leftarrow \mathbf{w} + \hat{\mathbf{a}}$

The procedure to derive the random corruption vector under the Monte-Carlo estimation of the indicator is shown in Algorithm 1. The correctness and randomness of the resulting corruption vector are assured and the theoretical results are given in Appendix. Without losing generality, we discuss the characteristics of the loss change caused by random corruption under a representative corruption constraint in Theorem 1. A detailed version of the theorem and the proof can be found in Appendix.

Theorem 1 (Distribution of Random Corruption). *Given the constraint set $S = \{\mathbf{a} : \|\mathbf{a}\|_2 = \epsilon\}$ and a generated random corruption $\tilde{\mathbf{a}}$ by Eq. (4), which in turn obeys a uniform distribution on $\|\tilde{\mathbf{a}}\|_2 = \epsilon$. The first-order estimation of $\Delta_{\max} \mathcal{L}(\mathbf{w}, S, \mathcal{D})$ and the expectation of the loss change caused by random corruption is*

$$\Delta_{\max} \mathcal{L}(\mathbf{w}, S, \mathcal{D}) = \epsilon G + o(\epsilon), \text{ and } \mathbb{E}_{\|\tilde{\mathbf{a}}\|_2 = \epsilon} [\Delta \mathcal{L}(\mathbf{w}, \tilde{\mathbf{a}}; \mathcal{D})] = O\left(\frac{\text{tr}(H)}{k} \epsilon^2\right). \quad (5)$$

Define $\eta = |\tilde{\mathbf{a}}^T \mathbf{g}| / \epsilon G$, which is an estimation of $|\Delta \mathcal{L}(\mathbf{w}, \tilde{\mathbf{a}}, \mathcal{D})| / \Delta_{\max} \mathcal{L}(\mathbf{w}, S, \mathcal{D})$, then $\eta \in [0, 1]$ and the probability density function $p_\eta(x)$ of η and the cumulative density $P(\eta \leq x)$ function of η are

$$p_\eta(x) = \frac{2\Gamma(\frac{k}{2})}{\sqrt{\pi}\Gamma(\frac{k-1}{2})} (1-x^2)^{\frac{k-3}{2}}, \text{ and } P(\eta \leq x) = \frac{2xF_1(\frac{1}{2}, \frac{3-k}{2}; \frac{3}{2}; x^2)}{B(\frac{k-1}{2}, \frac{1}{2})}, \quad (6)$$

where k denotes the number of corrupted parameters and $\Gamma(\cdot)$, $B(\cdot, \cdot)$ and $F_1(\cdot, \cdot; \cdot; \cdot)$ denote the gamma function, beta function and hyper-geometric function, respectively.

Theorem 1 states that the expectation of loss change of random corruption is infinitesimal compared to $\Delta_{\max} \mathcal{L}(\mathbf{w}, S, \mathcal{D})$ when $\epsilon \rightarrow 0$. In addition, it is unlikely for multiple random trials to induce the optimal loss change corresponding to the indicator. For a deep neural network, the number of parameters, which is the upper bound of k , can be considerably large. According to Eq.(6), η will be concentrated near 0. Thus, theoretically, it is not generally possible for the random corruption to cause substantial loss changes in this circumstance, making it ineffective in finding vulnerability.

2.2 Gradient-Based Corruption

To arrive at the optimal parameter corruption that renders a more accurate estimation of the proposed indicator, we further propose a gradient-based method based on maximizing the first-order estimation $f(\mathbf{a}) = \mathbf{a}^T \mathbf{g}$ of the indicator.

Definition 4 (Gradient-Based Corruption and Estimation). *Maximizing the first-order estimation $f(\mathbf{a}) = \mathbf{a}^T \mathbf{g}$ of the indicator, the gradient-based parameter corruption $\hat{\mathbf{a}}$ in S is*

$$\hat{\mathbf{a}} = \arg \max_{\mathbf{a} \in S} \mathbf{a}^T \mathbf{g} = \epsilon \left(\text{sgn}(\mathbf{h}) \odot \frac{|\mathbf{h}|^{\frac{1}{p-1}}}{\|\mathbf{h}\|^{\frac{1}{p-1}}\|_p} \right), \text{ and } f(\hat{\mathbf{a}}) = \hat{\mathbf{a}}^T \mathbf{g} = \epsilon \|\mathbf{h}\|^{\frac{p}{p-1}}, \quad (7)$$

where $\mathbf{h} = \text{top}_n(\mathbf{g})$, other notations are used similarly to Definition 3. The resultant corruption vector leads to a gradient-based estimation of the indicator.

The procedure of the gradient-based method is summarized in Algorithm 2. The error bound of the gradient-based estimation is described in Theorem 2. The proof and further analysis of computational complexity are provided in Appendix.

Theorem 2 (Error Bound of the Gradient-Based Estimation). *Suppose $\mathcal{L}(\mathbf{w}; \mathcal{D})$ is convex and L -smooth with respect to \mathbf{w} in the subspace $\{\mathbf{w} + \mathbf{a} : \mathbf{a} \in S\}$, where $S = \{\mathbf{a} : \|\mathbf{a}\|_p = \epsilon \text{ and } \|\mathbf{a}\|_0 \leq n\}$.² Suppose \mathbf{a}^* and $\hat{\mathbf{a}}$ are the optimal corruption and the gradient-based corruption in S respectively.*

²Note that \mathcal{L} is only required to be convex and L -smooth in a neighbourhood of \mathbf{w} , instead of the entire \mathbb{R}^k .

$\|\mathbf{g}\|_2 = G > 0$. It is easy to verify that $\mathcal{L}(\mathbf{w} + \mathbf{a}^*; \mathcal{D}) \geq \mathcal{L}(\mathbf{w} + \hat{\mathbf{a}}; \mathcal{D}) > \mathcal{L}(\mathbf{w}; \mathcal{D})$. It can be proved that the loss change of the gradient-based corruption is the same order infinitesimal of that of the optimal parameter corruption:

$$\frac{\Delta_{\max} \mathcal{L}(\mathbf{w}, S; \mathcal{D})}{\Delta \mathcal{L}(\mathbf{w}, \hat{\mathbf{a}}; \mathcal{D})} = 1 + O\left(\frac{L n^{\max\{1/2-2/p, 1/p-1\}} \sqrt{k\epsilon}}{G}\right). \quad (8)$$

Theorem 2 guarantees when perturbations to model parameters are small enough, the gradient-based corruption can accurately estimate the indicator with small errors. In Eq. (8), the numerator is the proposed indicator, which is the maximum loss change caused by parameter corruption, and the denominator is the loss change with the parameter corruption generated by the gradient-based method. As we can see, when the p -norm ϵ of the corruption vector tends to zero, the term $O(\cdot)$ will also tend to zero such that the ratio becomes one, meaning the gradient-based method is an infinitesimal estimation of the indicator.

3 Experiments

We first empirically validate the effectiveness of the proposed gradient-based corruption compared to random corruption. Then, it is applied to evaluate the robustness of neural network parameters by scanning for vulnerability and counteract parameter corruption via adversarial training.

3.1 Experimental Settings

We use four widely-used tasks including benchmark datasets in CV and NLP and use diverse neural network architecture. On the image classification task, the base model is ResNet-34 [16], the datasets are CIFAR-10 [32] and ImageNet, and the evaluation metric is accuracy. On the machine translation task, the base model is Transformer provided by fairseq [27], the dataset is German-English translation dataset (De-En) [27, 28, 35], and the evaluation metric is BLEU score. On the language modeling task, the base model is LSTM following [23, 24], the dataset is the English Penn TreeBank (PTB-LM) [22], and the evaluation metric is Log Perplexity (Log PPL). On the dependency parsing task, the base model is MLP following [5], the dataset is the English Penn TreeBank dependency parsing (PTB-Parsing) [22], and the evaluation metric is Unlabeled Attachment Score (UAS). For the detailed experimental setup, please refer to Appendix.

3.2 Empirical Validation of Gradient-Based Corruption

The comparative results between the gradient-based corruption and the random corruption are shown in Figure 3 and Table 1. Figure 3 shows that parameter corruption under the corruption constraint can result in substantial accuracy degradation for different sorts of neural networks and the gradient-based parameter corruption requires smaller perturbation than the random parameter corruption. The gradient-based corruption works for smaller corruption length and causes more damage at the same corruption length. To conclude, the gradient-based corruption effectively defects model parameters with minimal corruption length compared to the random corruption, thus being a viable and efficient approach to find the parameter vulnerability.

3.3 Probing the Vulnerability of DNN Parameters

Here we use the indicator to probe the Vulnerability of DNN Parameters. We use the gradient-based corruption on parameters from separated components and set n as the maximum number of the corrupted parameters. We probe the vulnerability of network parameters in terms of two natural structural characteristics of deep neural networks: the type, e.g., whether they belong to embeddings or convolutions, and the position, e.g., whether they belong to lower layers or higher layers. Due to limited space, the results of different layers in neural networks corrupted with multiple ϵ and detailed visualization of the vulnerability of different components are shown in Appendix.

Vulnerability in Terms of Parameter Types Figure 4 (a-b) show the distinguished vulnerability of different selected components in ResNet-34 and Transformer. Several observations can be drawn from the results: (1) *Normalization layers are prone to parameter corruption.* The batch normalization

Table 1: Comparisons of gradient-based corruption and random corruption under the corruption constraint, with further study on the number n of parameters to be corrupted. Here, all parameters can be corrupted, that is, k stands for the total number of model parameters and $n = k$ means the number of changed parameters is not limited. \uparrow means the higher value the better accuracy and \downarrow means the opposite. \star denotes original scores without parameter corruption and scores close to the original score (difference less than 0.1).

Dataset	ImageNet (Acc \uparrow)		CIFAR-10 (Acc \uparrow)		PTB-LM (Log PPL \downarrow)		PTB-Parsing (UAS \uparrow)		De-En (BLEU \uparrow)			
Base model	ResNet-34				LSTM		MLP		Transformer			
w/o corruption	72.5 \star				94.3 \star				4.25 \star			
Approach	Random	Proposed	Random	Proposed	Random	Proposed	Random	Proposed	Random	Proposed		
$n=k, \epsilon=10^{-4}$	\star	62.2 (-10.3)	\star	93.3 (-1.0)	\star	\star	\star	\star	\star	35.21 (-0.12)		
$n=k, \epsilon=10^{-3}$	\star	22.2 (-50.3)	\star	36.1 (-58.2)	\star	\star	\star	80.6 (-6.7)	\star	33.62 (-1.71)		
$n=k, \epsilon=10^{-2}$	30.3 (-42.2)	0.1 (-72.4)	75.1 (-19.2)	10.0 (-84.3)	\star	4.52 (+0.27)	79.8 (-7.5)	6.1 (-81.2)	34.82 (-0.51)	0.17 (-35.16)		
$n=k, \epsilon=10^{-1}$	0.1 (-72.4)	0.1 (-72.4)	10.0 (-84.3)	10.0 (-84.3)	4.43 (+0.18)	13.25 (+9.00)	0.0 (-87.3)	0.0 (-87.3)	0.00 (-35.33)	0.00 (-35.33)		
$n=k, \epsilon=1$	0.1 (-72.4)	0.1 (-72.4)	10.0 (-84.3)	10.0 (-84.3)	32.21 (+27.96)	48.92 (+44.67)	0.0 (-87.3)	0.0 (-87.3)	0.00 (-35.33)	0.00 (-35.33)		
$n=100, \epsilon=10^{-2}$	\star	\star	\star	\star	\star	\star	\star	64.6 (-22.7)	\star	\star		
$n=100, \epsilon=10^{-1}$	\star	67.5 (-5.0)	\star	\star	\star	\star	\star	11.0 (-76.3)	\star	31.68 (-3.65)		
$n=100, \epsilon=1$	\star	0.1 (-72.4)	\star	\star	\star	\star	87.1 (-0.2)	0.0 (-87.3)	35.25 (-0.08)	0.00 (-35.33)		
$n=100, \epsilon=10^1$	0.2 (-72.3)	0.1 (-72.4)	77.1 (-17.2)	44.8 (-49.5)	\star	\star	31.9 (-55.4)	0.0 (-87.3)	11.58 (-23.75)	0.00 (-35.33)		
$n=100, \epsilon=10^2$	0.1 (-72.4)	0.1 (-72.4)	10.1 (-84.2)	9.6 (-84.7)	16.90 (+12.65)	23.55 (+19.30)	0.0 (-87.3)	0.0 (-87.3)	0.00 (-35.33)	0.00 (-35.33)		

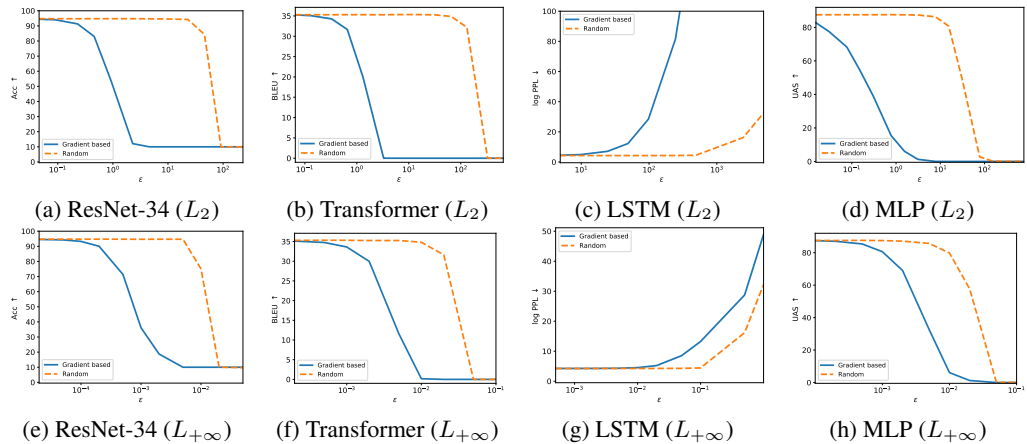


Figure 3: Results of gradient-based corruption and random corruption under the corruption constraints ($n = k$). Results of ResNet-34 are from CIFAR-10. We can conclude that the gradient-based corruption performs more effectively than the random corruption on all the tasks.

in ResNet-34 and the layer normalization in Transformer are most sensitive in comparison to other components in each network. It is possible that since these components adjust the data distribution, a slight change in scaling or biasing could lead to systematic disorder in the whole network. (2) *Convolution layers are more sensitive to corruption than fully-connected layers.* Since parameters in convolution, i.e., the filters, are repeatedly applied to the input feature grids, they might exert more influence than parameters in fully-connected layers that are only applied to the inputs once. (3) *Embedding and attention layers are relatively robust against parameter corruption.* It is obvious that embeddings consist of word vectors and fewer word vectors are corrupted if the corrupted number of parameters is limited, thus scarcely affecting the model. The robustness of attention is intriguing and further experimentation is required to understand its characteristics.

Vulnerability in Terms of Parameter Positions The illustration of division of different layers and results of parameter corruption on different layers are shown in Figure 4 (c-f). We can draw the following observations: (1) *Lower layers in ResNet-34 are less robust to parameter corruption.* It is generally believed that lower layers in convolutional neural networks extract basic visual patterns and are very fundamental in classification tasks [37], which indicates that perturbations to lower layers can fundamentally hurt the whole neural network. (2) *Upper layers in Transformer Decoder are less robust to parameter corruption.* From the sequence-to-sequence perspective, the encoder layers

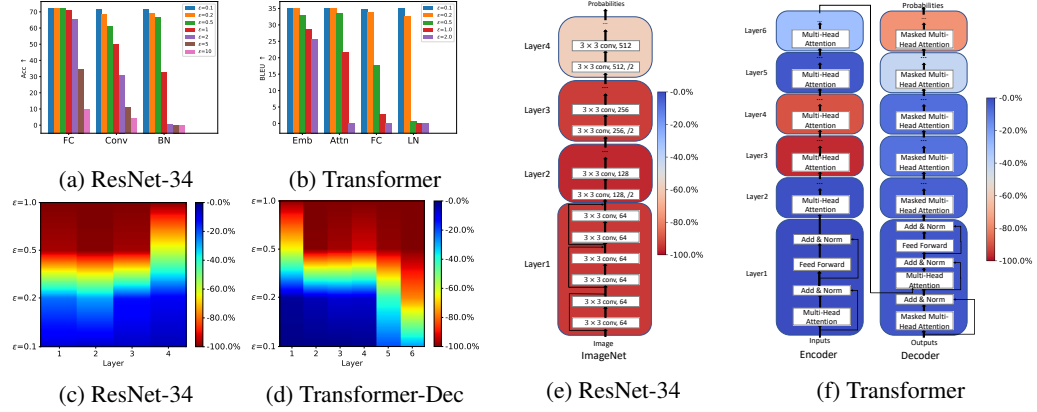


Figure 4: Results of gradient-based corruption on (a-b) different components of ResNet-34 (ImageNet) and Transformer under the corruption constraint ($p = +\infty, n = 10$) and (c-f) different layers in ResNet-34 and Transformer ($p = +\infty, n = 100$). Conv: convolution; Emb: embedding; FC: fully-connected; Attn: attention; BN: batch normalization; LN: layer normalization. ϵ is set to be 10 and 0.2 for ResNet-34 and Transformer, respectively. Warmer colors indicate significant accuracy degradation (compared to scores without parameter corruption in Table 1).

encode the sequence from shallow semantics to deep semantics and the decoder layers decode the sequence in a reversed order. It means that the higher layers are responsible for the choice of specific words and have a direct impact on the generated sequence. For Transformer Encoder, the parameter corruption exhibits inconspicuous trends.

As we can see, the proposed indicator reveals several problems that are rarely paid attention to before. Especially, the results on normalization layers should provide experimental verification for the heuristic designs of future architecture.

3.4 Improving Accuracy via Adversarial Corruption-Resistant Training

As shown by the probing results, the indicator can reveal interesting vulnerability of neural networks, which leads to poor robustness against parameter corruption. An important question is what we could do about the discovered vulnerability in practice, since it could be the innate characteristic of the neural network components and cannot be eliminated in design. However, if we can automatically drive the parameters from the area with steep surroundings measured by the indicator, we can obtain models that achieve natural balance on accuracy and parameter robustness.

To this end, we propose to counteract the parameter corruption in an adversarial way. The key idea is to routinely corrupt the parameters and minimize both the induced loss change and the original loss. Intuitively, the corruption-resistant training tries to keep the parameters away from the neighborhood where there are sheer directions around, which means the parameters should be situated at the center of a flattish basin in the loss landscape.

Concretely, given batched data \mathcal{B} , *virtual* gradient-based corruption $\hat{\mathbf{a}}$ on parameter \mathbf{w} , let's consider a new loss \mathcal{L}' that minimizes both the loss with corrupted parameter $\mathbf{w} + \hat{\mathbf{a}}$ and the initial loss:

$$\mathcal{L}'(\mathbf{w}; \mathcal{B}) = (1 - \lambda_1)\mathcal{L}(\mathbf{w}; \mathcal{B}) + \lambda_1\mathcal{L}(\mathbf{w} + \hat{\mathbf{a}}; \mathcal{B}) \approx \mathcal{L}(\mathbf{w}; \mathcal{B}) + \lambda_1 f(\hat{\mathbf{a}}). \quad (9)$$

Denote $\lambda_1 f(\hat{\mathbf{a}})$ as $\mathcal{R}(\mathbf{w}; \mathcal{B})$, which can be seen as a regularization term in the proposed adversarial corruption-resistant training. We can see that it actually serves as *gradient regularization* by simple derivation. Define $\lambda = \lambda_1 \epsilon$. According to Eq. (7), when $S = \{\|\mathbf{a}\|_p = \epsilon\}$, the regularization term is $\mathcal{R}(\mathbf{w}; \mathcal{B}) = \lambda_1 \epsilon \|\mathbf{g}\|_{p/(p-1)} = \lambda \|\mathbf{g}\|_{p/(p-1)}$.

Experimental Results We conduct experiments on CIFAR-10 and PTB-Parsing to validate that the proposed corruption-resistant training functions as designed. In experiments, we use $p = 2$ for CIFAR-10 and PTB-Parsing. In Table 2, we can see that incorporating a virtual gradient-based corruption into adversarial anti-corruption training can help improve both the accuracy of the uncorrupted model and the robustness of neural networks against parameter corruption. In particular, by comparing the

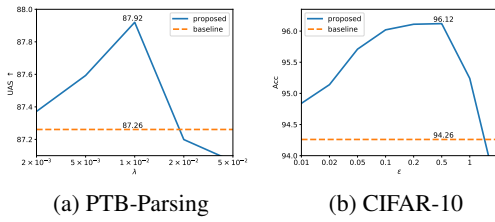


Figure 5: Results of corruption-resistant training with different ϵ or λ .

Table 2: Results of the proposed corruption-resistant training, which not only improves the accuracy without corruption but also enhances the robustness against corruption.

PTB-Parsing (UAS \uparrow)			CIFAR-10 (Acc \uparrow)		
\mathcal{L} /UAS	Baseline	Proposed	\mathcal{L} /Acc	Baseline	Proposed
UAS	87.26	87.92 (+0.66)	Acc	94.26	96.12 (+1.86)
\mathcal{L}	0.0807	0.0813	\mathcal{L}	0.0197	0.0203
$\epsilon=0.02$	80.82	86.37	$\epsilon=0.05$	93.20	95.65
$\epsilon=0.05$	72.04	80.75	$\epsilon=0.1$	89.84	94.59
$\epsilon=0.1$	57.42	71.70	$\epsilon=0.2$	71.44	87.92
$\epsilon=0.2$	37.94	55.40	$\epsilon=0.5$	13.77	21.42
$\epsilon=0.5$	0.00	2.70	$\epsilon=1$	10.00	10.94

loss, we can see that parameters that are resistant to corruption, albeit having higher training loss, may entail better generalization, reflected as higher accuracy in testing. In Figure 5, we show the influence of hyper-parameter λ to the accuracy. Based on the results, the accuracy of the uncorrupted neural network can often be improved substantially with small λ . In particular, the accuracy can be treated as a unimodal function of λ approximately, whose best configuration can be determined easily, showing general effectiveness of the proposed training approach.

4 Related Work

Vulnerability of DNNs Existing studies concerning vulnerability or robustness of neural networks mostly focus on generating adversarial examples [14] and adversarial training algorithms given adversarial examples in the input data [38]. [31] first proposed the concept of adversarial examples and found that neural network classifiers are vulnerable to adversarial attacks on input data. Following that study, different adversarial attack algorithms [26, 18] were developed. Another class of studies [7, 6, 15, 19] known as backdoor attacks injected vulnerabilities to neural networks by data poisoning, which requires access to the training process of the neural network models.

Adversarial Training Other related work on adversarial examples aimed to design adversarial defense algorithms to evaluate and improve the robustness of neural networks over adversarial examples [3, 21, 38]. As another application of adversarial training, GAN [13] has been widely used in multiple machine learning tasks, such as computer vision [10, 20, 33], natural language processing [12, 36, 8] and time series synthesis [9, 11]. It consists of a generator and a discriminator, where the generator aims to generate adversarial examples against the discriminator to generate synthetic and new instances of data.

To summarize, existing related work mostly focuses on adversarial examples and its adversarial training. However, we focus on parameter corruptions of neural networks so as to find vulnerable components of models and design an adversarial corruption-resistant training algorithm to improve the parameter robustness.

5 Conclusions

To better understand the vulnerability of DNN parameters, which is not well studied before, we propose an indicator measuring the maximum loss change when a small perturbation is applied to model parameters to evaluate the robustness against parameter corruption. Intuitively, the indicator describes the steepness of the loss surface around the parameters. We show that the indicator can be efficiently estimated by a gradient-based method and random parameter corruptions can hardly induce the maximum degradation, which is validated both theoretically and empirically. In addition, we apply the proposed indicator to systematically analyze the vulnerability of different parameters in different neural networks and reveal that the normalization layers, which are important in stabilizing the data distribution in deep neural networks, are prone to parameter corruption. Furthermore, we propose an adversarial learning approach to improve the parameter robustness and show that parameters that are resistant to parameter corruption embody better robustness and accuracy.

References

- [1] Abdelsalam, A.M., Boulet, F., Demers, G., Langlois, J.M.P., Cheriet, F.: An efficient fpga-based overlay inference architecture for fully connected dnns. In: 2018 International Conference on ReConfigurable Computing and FPGAs (ReConFig). pp. 1–6 (2018)
- [2] Bui, T.T.T., Phillips, B.: A scalable network-on-chip based neural network implementation on fpgas. In: 2019 IEEE-RIVF International Conference on Computing and Communication Technologies (RIVF). pp. 1–6 (2019)
- [3] Carlini, N., Wagner, D.A.: Towards evaluating the robustness of neural networks. In: 2017 IEEE Symposium on Security and Privacy, SP 2017, San Jose, CA, USA, May 22-26, 2017. pp. 39–57 (2017). <https://doi.org/10.1109/SP.2017.49>
- [4] Chaudhari, P., Choromanska, A., Soatto, S., LeCun, Y., Baldassi, C., Borgs, C., Chayes, J.T., Sagun, L., Zecchina, R.: Entropy-sgd: Biasing gradient descent into wide valleys. In: 5th International Conference on Learning Representations, ICLR 2017, Toulon, France, April 24-26, 2017, Conference Track Proceedings. OpenReview.net (2017), <https://openreview.net/forum?id=B1YfAfcl>
- [5] Chen, D., Manning, C.D.: A fast and accurate dependency parser using neural networks. In: Proceedings of the 2014 Conference on Empirical Methods in Natural Language Processing, EMNLP 2014, October 25-29, 2014, Doha, Qatar, A meeting of SIGDAT, a Special Interest Group of the ACL. pp. 740–750 (2014)
- [6] Chen, X., Liu, C., Li, B., Lu, K., Song, D.: Targeted backdoor attacks on deep learning systems using data poisoning. CoRR **abs/1712.05526** (2017), <http://arxiv.org/abs/1712.05526>
- [7] Dai, J., Chen, C., Li, Y.: A backdoor attack against lstm-based text classification systems. IEEE Access **7**, 138872–138878 (2019)
- [8] Dai, Z., Yang, Z., Yang, F., Cohen, W.W., Salakhutdinov, R.: Good semi-supervised learning that requires a bad GAN. In: Advances in Neural Information Processing Systems 30: Annual Conference on Neural Information Processing Systems 2017, 4-9 December 2017, Long Beach, CA, USA. pp. 6510–6520 (2017)
- [9] Donahue, C., McAuley, J.J., Puckette, M.S.: Synthesizing audio with generative adversarial networks. CoRR **abs/1802.04208** (2018)
- [10] Dziugaite, G.K., Roy, D.M., Ghahramani, Z.: Training generative neural networks via maximum mean discrepancy optimization. In: Proceedings of the Thirty-First Conference on Uncertainty in Artificial Intelligence, UAI 2015, July 12-16, 2015, Amsterdam, The Netherlands. pp. 258–267 (2015)
- [11] Esteban, C., Hyland, S.L., Rätsch, G.: Real-valued (medical) time series generation with recurrent conditional gans. CoRR **abs/1706.02633** (2017)
- [12] Fedus, W., Goodfellow, I.J., Dai, A.M.: Maskgan: Better text generation via filling in the _____. In: 6th International Conference on Learning Representations, ICLR 2018, Vancouver, BC, Canada, April 30 - May 3, 2018, Conference Track Proceedings (2018)
- [13] Goodfellow, I.J., Pouget-Abadie, J., Mirza, M., Xu, B., Warde-Farley, D., Ozair, S., Courville, A.C., Bengio, Y.: Generative adversarial networks. CoRR **abs/1406.2661** (2014)
- [14] Goodfellow, I.J., Shlens, J., Szegedy, C.: Explaining and harnessing adversarial examples. In: 3rd International Conference on Learning Representations, ICLR 2015, San Diego, CA, USA, May 7-9, 2015, Conference Track Proceedings (2015)
- [15] Gu, T., Liu, K., Dolan-Gavitt, B., Garg, S.: Badnets: Evaluating backdooring attacks on deep neural networks. IEEE Access **7**, 47230–47244 (2019). <https://doi.org/10.1109/ACCESS.2019.2909068>
- [16] He, K., Zhang, X., Ren, S., Sun, J.: Deep residual learning for image recognition. In: Proceedings of the IEEE conference on computer vision and pattern recognition. pp. 770–778 (2016)
- [17] Keskar, N.S., Mudigere, D., Nocedal, J., Smelyanskiy, M., Tang, P.T.P.: On large-batch training for deep learning: Generalization gap and sharp minima. In: 5th International Conference on Learning Representations, ICLR 2017, Toulon, France, April 24-26, 2017, Conference Track Proceedings. OpenReview.net (2017), <https://openreview.net/forum?id=H1oyR1Ygg>

[18] Kurakin, A., Goodfellow, I.J., Bengio, S.: Adversarial examples in the physical world. In: 5th International Conference on Learning Representations, ICLR 2017, Toulon, France, April 24-26, 2017, Workshop Track Proceedings (2017)

[19] Kurita, K., Michel, P., Neubig, G.: Weight poisoning attacks on pre-trained models. CoRR **abs/2004.06660** (2020), <https://arxiv.org/abs/2004.06660>

[20] Ma, L., Jia, X., Sun, Q., Schiele, B., Tuytelaars, T., Gool, L.V.: Pose guided person image generation. In: Advances in Neural Information Processing Systems 30: Annual Conference on Neural Information Processing Systems 2017, 4-9 December 2017, Long Beach, CA, USA. pp. 406–416 (2017)

[21] Madry, A., Makelov, A., Schmidt, L., Tsipras, D., Vladu, A.: Towards deep learning models resistant to adversarial attacks. In: 6th International Conference on Learning Representations, ICLR 2018, Vancouver, BC, Canada, April 30 - May 3, 2018, Conference Track Proceedings (2018)

[22] Marcus, M.P., Santorini, B., Marcinkiewicz, M.A.: Building a large annotated corpus of english: The penn treebank. Computational Linguistics **19**(2), 313–330 (1993)

[23] Merity, S., Keskar, N.S., Socher, R.: Regularizing and Optimizing LSTM Language Models. arXiv preprint arXiv:1708.02182 (2017)

[24] Merity, S., Keskar, N.S., Socher, R.: An Analysis of Neural Language Modeling at Multiple Scales. arXiv preprint arXiv:1803.08240 (2018)

[25] Misra, J., Saha, I.: Artificial neural networks in hardware: A survey of two decades of progress. Neurocomputing **74**(1-3), 239–255 (2010). <https://doi.org/10.1016/j.neucom.2010.03.021>, <https://doi.org/10.1016/j.neucom.2010.03.021>

[26] Moosavi-Dezfooli, S., Fawzi, A., Frossard, P.: Deepfool: A simple and accurate method to fool deep neural networks. In: 2016 IEEE Conference on Computer Vision and Pattern Recognition, CVPR 2016, Las Vegas, NV, USA, June 27-30, 2016. pp. 2574–2582 (2016). <https://doi.org/10.1109/CVPR.2016.282>

[27] Ott, M., Edunov, S., Baevski, A., Fan, A., Gross, S., Ng, N., Grangier, D., Auli, M.: fairseq: A fast, extensible toolkit for sequence modeling. arXiv preprint arXiv:1904.01038 (2019)

[28] Ranzato, M., Chopra, S., Auli, M., Zaremba, W.: Sequence level training with recurrent neural networks. In: 4th International Conference on Learning Representations, ICLR 2016, San Juan, Puerto Rico, May 2-4, 2016, Conference Track Proceedings (2016)

[29] Russakovsky, O., Deng, J., Su, H., Krause, J., Satheesh, S., Ma, S., Huang, Z., Karpathy, A., Khosla, A., Bernstein, M.S., Berg, A.C., Li, F.: Imagenet large scale visual recognition challenge. Int. J. Comput. Vis. **115**(3), 211–252 (2015). <https://doi.org/10.1007/s11263-015-0816-y>, <https://doi.org/10.1007/s11263-015-0816-y>

[30] Salimi-Nezhad, N., Ilbeigi, E., Amiri, M., Falotico, E., Laschi, C.: A digital hardware system for spiking network of tactile afferents. Frontiers in Neuroscience **13** (2019)

[31] Szegedy, C., Zaremba, W., Sutskever, I., Bruna, J., Erhan, D., Goodfellow, I.J., Fergus, R.: Intriguing properties of neural networks. In: 2nd International Conference on Learning Representations, ICLR 2014, Banff, AB, Canada, April 14-16, 2014, Conference Track Proceedings (2014)

[32] Torralba, A., Fergus, R., Freeman, W.T.: 80 million tiny images: A large data set for non-parametric object and scene recognition. IEEE transactions on pattern analysis and machine intelligence **30**(11), 1958–1970 (2008)

[33] Vondrick, C., Pirsiavash, H., Torralba, A.: Generating videos with scene dynamics. In: Advances in Neural Information Processing Systems 29: Annual Conference on Neural Information Processing Systems 2016, December 5-10, 2016, Barcelona, Spain. pp. 613–621 (2016)

[34] Weber, T.O., da Silva Labres, D., Cabrera, F.L.: Amplifier-based mos analog neural network implementation and weights optimization. In: 2019 32nd Symposium on Integrated Circuits and Systems Design (SBCCI). pp. 1–6 (2019)

[35] Wiseman, S., Rush, A.M.: Sequence-to-sequence learning as beam-search optimization. In: Proceedings of the 2016 Conference on Empirical Methods in Natural Language Processing, EMNLP 2016, Austin, Texas, USA, November 1-4, 2016. pp. 1296–1306 (2016)

[36] Yang, Z., Hu, J., Salakhutdinov, R., Cohen, W.W.: Semi-supervised QA with generative domain-adaptive nets. In: Proceedings of the 55th Annual Meeting of the Association for Computational Linguistics, ACL 2017, Vancouver, Canada, July 30 - August 4, Volume 1: Long Papers. pp. 1040–1050 (2017). <https://doi.org/10.18653/v1/P17-1096>

[37] Yosinski, J., Clune, J., Bengio, Y., Lipson, H.: How transferable are features in deep neural networks? In: Advances in Neural Information Processing Systems 27: Annual Conference on Neural Information Processing Systems 2014. pp. 3320–3328 (2014)

[38] Zhu, C., Cheng, Y., Gan, Z., Sun, S., Goldstein, T., Liu, J.: Freelb: Enhanced adversarial training for language understanding. CoRR **abs/1909.11764** (2019)

A Appendix

A.1 Theoretical Analysis of the Random Corruption

In this section, we discuss the characteristics of the loss change caused by random corruption under a representative corruption constraint in Theorem 1. Here we choose the constraint set $S = \{\mathbf{a} : \|\mathbf{a}\|_2 = \epsilon\}$ and show that it is not generally possible for the random corruption to cause substantial loss changes in this circumstance both theoretically and experimentally, making it ineffective in finding vulnerability.

In Theorem 1, the detailed definitions of the gamma function, beta function and hyper-geometric function are as follows: $\Gamma(\cdot)$ and $B(\cdot, \cdot)$ denote the gamma function and beta function, and $F_1(\cdot, \cdot; \cdot; \cdot)$ denotes the Gaussian or ordinary hyper-geometric function, which can also be written as ${}_2F_1(\cdot, \cdot; \cdot; \cdot)$:

$$\Gamma(z) = \int_0^{+\infty} t^{z-1} e^{-t} dt, \quad B(p, q) = \int_0^1 t^{p-1} (1-t)^{q-1} dt, \quad (10)$$

$$F_1(a, b; c; z) = 1 + \sum_{n=1}^{+\infty} \frac{a(a+1) \cdots (a+n-1) \times b(b+1) \cdots (b+n-1)}{c(c+1) \cdots (c+n-1)} \frac{z^n}{n!}. \quad (11)$$

Theorem 1 states that the expectation of loss change of random corruption is infinitesimal compared to $\Delta_{\max} \mathcal{L}(\mathbf{w}, S, \mathcal{D})$ when $\epsilon \rightarrow 0$. In addition, it is unlikely for multiple random trials to induce the optimal loss change corresponding to the indicator. For a deep neural network, the number of parameters, which is the upper bound of k , can be considerably large. According to Eq.(6), η will be concentrated near 0. Thus, theoretically, it is not generally possible for the random corruption to cause substantial loss changes in this circumstance, making it ineffective in finding vulnerability.

The conclusion is also empirically validated. In particular, we define $\alpha(p)$ as a real number in $[0, 1]$ satisfying $P(|\Delta \mathcal{L}(\mathbf{w}, \tilde{\mathbf{a}}, \mathcal{D})| < \alpha(p)) = p$, which means $|\Delta \mathcal{L}(\mathbf{w}, \tilde{\mathbf{a}}, \mathcal{D})| < \alpha(p)$ keeps with a probability p . We then compare the gradient-based corruption and 10,000 random corruptions on a language model and ϵ is set to 5×10^{-4} . The distribution of the results of the 10,000 random corruptions are reported in Table 3, as well as the gradient-based corruption result. We can find that the gradient-based corruption can cause a loss change ϵG of 0.044, while the loss change of the random corruption $|\Delta \mathcal{L}(\mathbf{w}, \tilde{\mathbf{a}}, \mathcal{D})|$ is less than 10^{-4} with a high probability, which shows a huge difference of more than 400 times ($\eta < 1/400$) in terms of the corrupting effectiveness.

Table 3: Probability distribution of corruption effects $|\Delta \mathcal{L}(\mathbf{w}, \tilde{\mathbf{a}}, \mathcal{D})|$ for random corruption. $\alpha(p)$ satisfies $P(|\Delta \mathcal{L}(\mathbf{w}, \tilde{\mathbf{a}}, \mathcal{D})| < \alpha(p)) = p$. Random corruption has small loss changes with high probability while gradient-based corruption results in a loss change 400 times larger.

Approach	$\alpha(0.9)$	$\alpha(0.95)$	$\alpha(0.995)$
Random corruption (Empirical)	4.0×10^{-5}	4.8×10^{-5}	7.0×10^{-5}
Random corruption (Theoretical)	1.5×10^{-5}	1.8×10^{-5}	2.5×10^{-5}
gradient-based corruption			$\Delta_{\max} \mathcal{L}(\mathbf{w}, S, \mathcal{D}) \approx \epsilon G = 0.044$

A.2 Proofs

A.2.1 Proof of Theorem 1

Proof. According to Definition 3,

$$\tilde{\mathbf{a}} = \arg \max_{\|\mathbf{a}\|_2=\epsilon} \mathbf{a}^T \mathbf{r} = \epsilon \frac{\mathbf{r}}{\|\mathbf{r}\|_2} \quad (12)$$

where $\mathbf{r} \sim N(0, 1)$ ($1 \leq i \leq k$). Note that \mathbf{r} obeys the Gaussian distribution with a mean vector of zero and a covariance matrix of I . Thus, the distribution of \mathbf{r} has rotational invariance and $\tilde{\mathbf{a}} = \epsilon \frac{\mathbf{r}}{\|\mathbf{r}\|_2}$ also has rotational invariance. Therefore, $\tilde{\mathbf{a}}$ obeys a uniform distribution on $\|\tilde{\mathbf{a}}\|_2 = \epsilon$.

First, we proof Eq.(5).

$$\Delta \mathcal{L}(\mathbf{w}, \mathbf{a}; \mathcal{D}) = \mathbf{a}^T \mathbf{g} + \frac{1}{2} \mathbf{a}^T H \mathbf{a} + o(\epsilon^2) = f(\mathbf{a}) + o(\epsilon), \max_{\|\mathbf{a}\|_2=\epsilon} f(\mathbf{a}) = \max_{\|\mathbf{a}\|_2=\epsilon} \mathbf{a}^T = \epsilon G \quad (13)$$

Therefore,

$$\Delta_{\max} \mathcal{L}(\mathbf{w}, S, \mathcal{D}) = \epsilon G + o(\epsilon) \quad (14)$$

Suppose $\tilde{\mathbf{a}} = (a_1, a_2, \dots, a_{k-1}, a_k)^T$, $\mathbf{g} = (g_1, g_2, \dots, g_{k-1}, g_k)^T$ and $H_{ij} = \partial^2 \mathcal{L}(\mathbf{w} + \mathbf{a}; \mathcal{D}) / \partial a_i \partial a_j$. Since $\tilde{\mathbf{a}}$ obeys a uniform distribution on $\|\tilde{\mathbf{a}}\|_2 = \epsilon$, by symmetry, we have,

$$\mathbb{E}_{\|\tilde{\mathbf{a}}\|_2=\epsilon} [a_i] = \mathbb{E}_{\|\tilde{\mathbf{a}}\|_2=\epsilon} [a_i a_j] = 0 \quad (i \neq j) \quad (15)$$

$$\mathbb{E}_{\|\tilde{\mathbf{a}}\|_2=\epsilon} [a_i^2] = \mathbb{E}_{\|\tilde{\mathbf{a}}\|_2=\epsilon} \left[\frac{\|\mathbf{a}\|^2}{k} \right] = \frac{\epsilon^2}{k} \quad (16)$$

Therefore,

$$\mathbb{E}_{\|\tilde{\mathbf{a}}\|_2=\epsilon} [\Delta \mathcal{L}(\mathbf{w}, \tilde{\mathbf{a}}, \mathcal{D})] = \mathbb{E}_{\|\tilde{\mathbf{a}}\|_2=\epsilon} [\tilde{\mathbf{a}}^T \mathbf{g} + \frac{1}{2} \tilde{\mathbf{a}}^T H \tilde{\mathbf{a}} + o(\epsilon^2)] \quad (17)$$

$$= \mathbb{E}_{\|\tilde{\mathbf{a}}\|_2=\epsilon} [\tilde{\mathbf{a}}^T \mathbf{g}] + \mathbb{E}_{\|\tilde{\mathbf{a}}\|_2=\epsilon} \left[\frac{1}{2} \tilde{\mathbf{a}}^T H \tilde{\mathbf{a}} \right] + o(\epsilon^2) \quad (18)$$

$$= \mathbb{E}_{\|\tilde{\mathbf{a}}\|_2=\epsilon} \left[\sum_i g_i a_i \right] + \mathbb{E}_{\|\tilde{\mathbf{a}}\|_2=\epsilon} \left[\frac{1}{2} \sum_{i,j} H_{ij} a_i a_j \right] + o(\epsilon^2) \quad (19)$$

$$= \sum_i H_{ii} \frac{\epsilon^2}{2k} + o(\epsilon^2) \quad (20)$$

$$= O\left(\frac{\text{tr}(H)}{k} \epsilon^2\right) \quad (21)$$

Then, we proof Eq.(6). Because of the rotational invariance of the distribution of $\tilde{\mathbf{a}}$, we may assume $\frac{\mathbf{g}}{\|\mathbf{g}\|_2} = (1, 0, 0, \dots, 0)^T$, $\tilde{\mathbf{a}} = (a_1, a_2, a_3, \dots, a_{k-1}, a_k)^T$ and

$$\left\{ \begin{array}{l} a_1 = \epsilon \cos \phi_1 \\ a_2 = \epsilon \sin \phi_1 \cos \phi_2 \\ a_3 = \epsilon \sin \phi_1 \sin \phi_2 \cos \phi_3 \\ \dots \\ a_{k-1} = \epsilon \sin \phi_1 \sin \phi_2 \dots \sin \phi_{k-2} \cos \phi_{k-1} \\ a_k = \epsilon \sin \phi_1 \sin \phi_2 \dots \sin \phi_{k-2} \sin \phi_{k-1} \end{array} \right. \quad (22)$$

where $\phi_i \in [0, \pi]$ ($i \neq k-1$) and $\phi_{k-1} \in [0, 2\pi]$. For $x \in [0, 1]$, define $\alpha = \arccos x$, then:

$$f(\tilde{\mathbf{a}}) = \tilde{\mathbf{a}}^T \mathbf{g} = \epsilon G \cos \phi_1, P(\eta \leq x) = P(|\cos \phi_1| \leq x) = 2P(0 \leq \phi_1 \leq \alpha) \quad (23)$$

That is to say,

$$P(\eta \leq x) = \frac{2 \int_0^{2\pi} \int_0^\pi \cdots \int_0^\alpha (\sin^{k-2} \phi_1 \sin^{k-3} \phi_2 \cdots \sin \phi_{k-2}) d\phi_1 \cdots d\phi_{k-2} d\phi_{k-1}}{\int_0^{2\pi} \int_0^\pi \cdots \int_0^\pi (\sin^{k-2} \phi_1 \sin^{k-3} \phi_2 \cdots \sin \phi_{k-2}) d\phi_1 \cdots d\phi_{k-2} d\phi_{k-1}} \quad (24)$$

$$= \frac{2 \int_0^\alpha \sin^{k-2} \phi_1 d\phi_1}{\int_0^\pi \sin^{k-2} \phi_1 d\phi_1} = \frac{\int_0^\alpha \sin^{k-2} \phi_1 d\phi_1}{\int_0^{\frac{\pi}{2}} \sin^{k-2} \phi_1 d\phi_1} = \frac{2 \int_0^\alpha \sin^{k-2} \phi_1 d\phi_1}{B(\frac{k-1}{2}, \frac{1}{2})} \quad (25)$$

$$= \frac{2 \cos \alpha F_1(\frac{1}{2}, \frac{3-k}{2}; \frac{3}{2}; \cos^2 \alpha)}{B(\frac{k-1}{2}, \frac{1}{2})} = \frac{2x F_1(\frac{1}{2}, \frac{3-k}{2}; \frac{3}{2}; x^2)}{B(\frac{k-1}{2}, \frac{1}{2})} \quad (26)$$

and notice that

$$\sin \alpha = (1 - x^2)^{\frac{1}{2}}, \left| \frac{d\alpha}{dx} \right| = \frac{1}{(1 - x^2)^{\frac{1}{2}}}, B(p, q) = \frac{\Gamma(p)\Gamma(q)}{\Gamma(p+q)}, \Gamma(\frac{1}{2}) = \sqrt{\pi} \quad (27)$$

then according to Eq.(25):

$$p_\eta(x) = \frac{2 \sin^{k-2} \alpha}{B(\frac{k-1}{2}, \frac{1}{2})} \left| \frac{d\alpha}{dx} \right| = \frac{2\Gamma(\frac{k}{2})}{\sqrt{\pi}\Gamma(\frac{k-1}{2})} (1 - x^2)^{\frac{k-3}{2}} \quad (28)$$

□

A.2.2 Closed-Form Solutions in Definitions

The close-form solutions of the random parameter corruption in Definition 3 and gradient-based corruption in Definition 4 can be generalized into Proposition 1, which is the maximum of linear function under the corruption constraint.

Proposition 1 (Constrained Maximum). *Given a vector $\mathbf{v} \in \mathbb{R}^k$, the optimal $\hat{\mathbf{a}}$ that maximizes $\mathbf{a}^T \mathbf{v}$ under the corruption constraint $\mathbf{a} \in S = \{\mathbf{a} : \|\mathbf{a}\|_p = \epsilon \text{ and } \|\mathbf{a}\|_0 \leq n\}$ is*

$$\hat{\mathbf{a}} = \arg \max_{\mathbf{a} \in S} \mathbf{a}^T \mathbf{v} = \epsilon (\text{sgn}(\mathbf{h}) \odot \frac{|\mathbf{h}|^{\frac{1}{p-1}}}{\|\mathbf{h}\|^{\frac{1}{p-1}}}), \text{ and } \hat{\mathbf{a}}^T \mathbf{v} = \epsilon \|\mathbf{h}\|_{\frac{p}{p-1}}, \quad (29)$$

where $\mathbf{h} = \text{top}_n(\mathbf{v})$, retaining top- n magnitude of all $|\mathbf{v}|$ dimensions and set other dimensions to 0, $\text{sgn}(\cdot)$ denotes the signum function, $|\cdot|$ denotes the point-wise absolute function, and $(\cdot)^\alpha$ denotes the point-wise α -power function.

Proof. When $\mathbf{a} \in S = \{\mathbf{a} : \|\mathbf{a}\|_p = \epsilon \text{ and } \|\mathbf{a}\|_0 \leq n\}$, define $\mathbf{a} = P\mathbf{b}$, where P is a diagonal 0/1 matrix with n ones. It is easy to verify $P^T = P = P^2$. Define $q = \frac{p}{p-1}, \frac{1}{p} + \frac{1}{q} = 1$ here. Then according to Holder Inequality, for $\frac{1}{p} + \frac{1}{q} = 1, (1 \leq p, q \leq +\infty)$,

$$\mathbf{a}^T \mathbf{v} = \mathbf{b}^T P \mathbf{v} = \mathbf{b}^T P P \mathbf{v} = \mathbf{a}^T (P \mathbf{v}) \leq \|\mathbf{a}\|_p \|P \mathbf{v}\|_q = \epsilon \|\mathbf{h}\|_{\frac{p}{p-1}} \quad (30)$$

where $\mathbf{h} = M\mathbf{v} = \text{top}_n(\mathbf{v})$, M is a diagonal 0/1 matrix and $M_{j,j} = 1$ if and only if $|\mathbf{v}|_j$ is in the top- n magnitude of all $|\mathbf{v}|$ dimensions. The equation holds if and only if,

$$\hat{\mathbf{a}} = \epsilon (\text{sgn}(\mathbf{h}) \odot \frac{|\mathbf{h}|^{\frac{1}{p-1}}}{\|\mathbf{h}\|^{\frac{1}{p-1}}}) \quad (31)$$

and the maximum value of $\mathbf{a}^T \mathbf{v}$ is $\hat{\mathbf{a}}^T \mathbf{v} = \epsilon \|\mathbf{h}\|_{\frac{p}{p-1}}$. □

Proposition 1 indicates that the maximization of the value $\mathbf{a}^T \mathbf{v}$ under the corruption constraint has a closed-form solution. The solutions to a special case, where $p = +\infty$ are shown below.

Corollary 1. *When $p = +\infty$, the solution in Proposition 1 is,*

$$\hat{\mathbf{a}} = \lim_{p \rightarrow +\infty} \epsilon (\text{sgn}(\mathbf{h}) \odot \frac{|\mathbf{h}|^{\frac{1}{p-1}}}{\|\mathbf{h}\|^{\frac{1}{p-1}}}) = \epsilon \text{sgn}(\mathbf{h}), \text{ and } \hat{\mathbf{a}}^T \mathbf{v} = \epsilon \|\mathbf{h}\|_1 \quad (32)$$

Proof. In Proposition 1, when $p \rightarrow +\infty$, $0^{\frac{1}{p-1}} \rightarrow 0$, $x^{\frac{1}{p-1}} \rightarrow 1$ ($x \neq 0$) and $|\mathbf{h}|^{\frac{1}{p-1}} \rightarrow \mathbb{I}(\mathbf{h} \neq 0)$. Then

$$\hat{\mathbf{a}} = \lim_{p \rightarrow +\infty} \epsilon(\text{sgn}(\mathbf{h}) \odot \frac{|\mathbf{h}|^{\frac{1}{p-1}}}{\|\mathbf{h}\|^{\frac{1}{p-1}}}) = \epsilon \text{sgn}(\mathbf{h}) \quad (33)$$

and the maximum value of $\mathbf{a}^T \mathbf{v}$ is $\hat{\mathbf{a}}^T \mathbf{v} = \epsilon \|\mathbf{h}\|_{\frac{p}{p-1}} = \epsilon \|\mathbf{h}\|_1$.

□

A.2.3 Proof of Theorem 2

Proof. Define $q = \frac{p}{p-1}$, $\frac{1}{p} + \frac{1}{q} = 1$ here.

We introduce a lemma first.

Lemma A.1. For vector $\mathbf{x} \in \mathbb{R}^k$, $\|\mathbf{x}\|_0 \leq n \leq k$, for any $r > 1$, $\|\mathbf{x}\|_2 \leq \beta_r \|\mathbf{x}\|_r$, where $\beta_r = \max\{1, n^{1/2-1/r}\}$.

Proof of Lemma A.1. We may assume $\mathbf{x} = (x_1, x_2, \dots, x_k)^T$ and $x_{n+1} = x_{n+2} = \dots = x_k = 0$.

Then $\|\mathbf{x}\|_r = \left(\sum_{i=1}^n |x_i|^r \right)^{\frac{1}{r}}$.

When $1 < r < 2$, define $t = \frac{r}{2} < 1$ and $h(x) = x^t + (1-x)^t$, $h''(x) = t(t-1)(x^{t-2} + (1-x)^{t-2}) < 0$, thus $h(x) \geq \max\{h(0), h(1)\} = 1$ ($x \in [0, 1]$).

Then for $a, b \geq 0$ and $a + b > 0$, we have $\frac{a^t + b^t}{(a+b)^t} = \left(\frac{a}{a+b}\right)^t + \left(1 - \frac{a}{a+b}\right)^t = h\left(\frac{a}{a+b}\right) \geq 1$. That is to say, $a^t + b^t \geq (a+b)^t$. More generally, $a^t + b^t + \dots + c^t \geq (a+b+\dots+c)^t$. Therefore,

$$\|\mathbf{x}\|_r = \left(\sum_{i=1}^n |x_i|^r \right)^{\frac{1}{r}} = \left(\sum_{i=1}^n (|x_i|^2)^{\frac{r}{2}} \right)^{\frac{1}{r}} \geq \left(\left(\sum_{i=1}^n |x_i|^2 \right)^{\frac{r}{2}} \right)^{\frac{1}{r}} = \|\mathbf{x}\|_2 \quad (34)$$

When $r \geq 2$, according to the power mean inequality,

$$\|\mathbf{x}\|_r = \left(\sum_{i=1}^n |x_i|^r \right)^{\frac{1}{r}} = n^{\frac{1}{r}} \left(\frac{\sum_{i=1}^n |x_i|^r}{n} \right)^{\frac{1}{r}} \geq n^{\frac{1}{r}} \left(\frac{\sum_{i=1}^n |x_i|^2}{n} \right)^{\frac{1}{2}} = n^{\frac{1}{r}-\frac{1}{2}} \left(\sum_{i=1}^n |x_i|^2 \right)^{\frac{1}{2}} = n^{\frac{1}{r}-\frac{1}{2}} \|\mathbf{x}\|_2 \quad (35)$$

To conclude, $\|\mathbf{x}\|_2 \leq \beta_r \|\mathbf{x}\|_r$, where $\beta_r = \max\{1, n^{1/2-1/r}\}$.

□

According to Lemma A.1, notice that $\|\mathbf{a}^*\|_0 \leq n$, define $\mathbf{h} = \text{top}_n(\mathbf{g})$, then $\|\mathbf{h}\|_2 \geq \frac{n}{k} \|\mathbf{g}\|_2$ we have,

$$\|\mathbf{a}^*\|_2 \leq \beta_p \|\mathbf{a}^*\|_p \leq \beta_p \epsilon, \quad \|\mathbf{h}\|_q \geq \frac{\|\mathbf{h}\|_2}{\beta_q} \sqrt{\frac{n}{k}} = \frac{G}{\beta_q} \sqrt{\frac{n}{k}} \quad (36)$$

Since $\mathcal{L}(\mathbf{w}; \mathcal{D})$ is convex and L -smooth in $\mathbf{w} + S$,

$$\Delta \mathcal{L}(\mathbf{w}, \hat{\mathbf{a}}, \mathcal{D}) \geq \mathbf{g}^T \hat{\mathbf{a}} = \epsilon \|\mathbf{h}\|_q \quad (37)$$

$$\Delta \mathcal{L}(\mathbf{w}, \mathbf{a}^*, \mathcal{D}) \leq \mathbf{g}^T \mathbf{a}^* + \frac{L}{2} \|\mathbf{a}^*\|_2^2 = \epsilon \|\mathbf{h}\|_q + \frac{L}{2} \|\mathbf{a}^*\|_2^2 \quad (38)$$

Therefore,

$$\text{Left Hand Side} = \frac{\Delta \mathcal{L}(\mathbf{w}, \mathbf{a}^*, \mathcal{D})}{\Delta \mathcal{L}(\mathbf{w}, \hat{\mathbf{a}}, \mathcal{D})} \leq \frac{\epsilon \|\mathbf{h}\|_q + \frac{L}{2} \|\mathbf{a}^*\|_2^2}{\epsilon \|\mathbf{h}\|_q} \leq 1 + \frac{L \beta_p^2 \epsilon}{2 \|\mathbf{h}\|_q} \leq 1 + \frac{L \beta_p^2 \beta_q \epsilon \sqrt{k}}{2G\sqrt{n}} \quad (39)$$

When $p \geq 2, q \leq 2$, $\beta_p^2 \beta_q = n^{1-2/p}$, and when $p \leq 2, q \geq 2$, $\beta_p^2 \beta_q = n^{1/2-1/q} = n^{1/p-1/2}$. To conclude, $\beta_p^2 \beta_q = \max\{n^{1-2/p}, n^{1/p-1/2}\} = n^{\max\{1-2/p, 1/p-1/2\}}$, therefore,

$$\text{Left Hand Side} \leq 1 + \frac{L n^{\max\{1-2/p, 1/p-1/2\}} \sqrt{k}}{2G\sqrt{n}} \epsilon = 1 + O\left(\frac{L n^{\max\{1/2-2/p, 1/p-1\}} \sqrt{k} \epsilon}{G}\right) \quad (40)$$

□

A.3 Computational Complexity of Parameter Corruption

For the parameter corruption, the closed-form solution is determined by (1) the set of allowed corruptions S , i.e., n, k, ϵ and p ; and (2) the vector \mathbf{v} , corresponding to \mathbf{r} in random corruption and \mathbf{g} in gradient-based corruption. The first condition has a computational cost of $O(k \log n)$, because a top- n check is involved, which is at least $O(k \log n)$, and other calculations, such as multiplication and inversion, are less than $O(k)$.

For the second condition, sampling \mathbf{r} should be trivial on modern computers but obtaining \mathbf{g} with respect to the whole dataset can be costly, generally of cost $O(k|\mathcal{D}|)$.

A.4 Model Implementation

This section shows the implementation details of neural networks used in our experiments. Experiments are conducted on a GeForce GTX TITAN X GPU.

A.4.1 ResNet

We adopt Resnet-34 [16] as a baseline on two benchmark datasets: CIFAR-10 [32] and ImageNet [29]. CIFAR-10³ is an image classification dataset with 10 categories and consists of 50000 training images and 10000 test images. The images are of 32-by-32 pixel size with 3 channels. We adopt the classification accuracy as our evaluation metric on CIFAR-10. For ImageNet⁴, it contains 10M labeled images of more than 10k categories as the training dataset and 50k images as the validation dataset. Note that the gradient-based parameter corruption on ResNet on ImageNet uses gradients from the validation set due to the sheer size of ImageNet, while other experiments use gradients from the training set. We adopt the Top-1 and Top-5 accuracy (Acc) on the validation dataset as our evaluation metrics on ImageNet. We adopt SGD as the optimizer with the mini-batch size of 128. The learning rate is 0.1; the momentum is 0.9; and the weight-decay is 5×10^{-4} . We also apply data augmentation for training following [16]: 4 pixels are padded on each side, and a 32*32 crop is randomly sampled from the padded image or its horizontal flip. In adversarial corruption-resistant training, we find that directly optimizing the new loss \mathcal{L}' in Eq. 9 instead of optimizing the regularization term can further improve the accuracy. Therefore we optimize \mathcal{L}' directly and choose $\lambda_1 = 0.5$. Here $\lambda \approx \lambda_1 \epsilon = \epsilon/2$, we report the hyper-parameter ϵ instead of λ in paper.

A.4.2 Transformer

We implement the “transformer_iwslt_de_en” provided by fairseq [27] on German-English translation dataset. We use the same dataset splits following [27, 28, 35]. The dataset and the implementation of “transformer_iwslt_de_en” can be found at the fairseq repository⁵. The dataset contains 153K sentences for training, 7K sentences for validation, and 7K sentences for testing. BPE is used to get vocabularies. We adopt BLEU score as the evaluation metric on the translation task. We use the shared embedding settings and adopt a vocabulary size of 10,149. The dropout rate is 0.3, the attention dropout rate is 0.1 and the activation dropout rate is 0.1. The training batch size is 4,096 tokens and we update the model for every 2 steps. We adopt a learning rate schedule with an initial learning rate of 10^{-7} and a base learning rate of 0.0015. The number of warmup steps is 8000. We set the test beam-size to 5. We adopt the checkpoint-average mechanism for evaluation and the last 10 checkpoints are averaged.

A.4.3 LSTM

We use a 3-layer LSTM as a language model following [23, 24] on the word-level Penn TreeBank dataset (PTB)⁶[22]. The dataset has been preprocessed and the vocabulary size is limited to 10000 words. We adopt the log perplexity on the test set as the evaluation metric on PTB. We use the Adam optimizer and initialize the learning rate with 0.001. The embedding size is set to 400 and the hidden size is set to 1150. We use the weight-decay of 1.2×10^{-6} .

³CIFAR-10 can be found at <https://www.cs.toronto.edu/~kriz/cifar.html>

⁴ImageNet can be found at <http://www.image-net.org>

⁵<https://github.com/pytorch/fairseq>

⁶PTB can be found at <https://www.kaggle.com/nltkdata/penn-tree-bank?select=ptb>

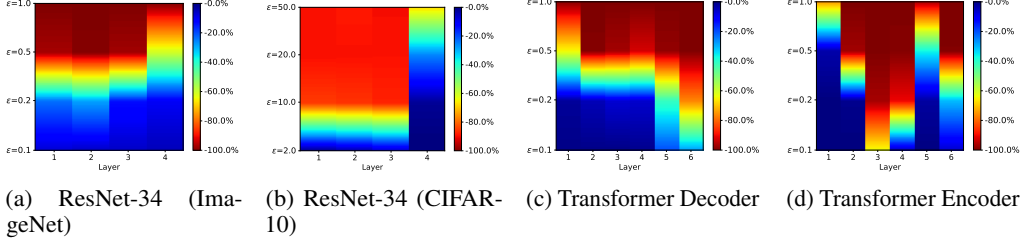


Figure 6: Results of gradient-based gradient-based corruption on different layers in ResNet-34 and Transformer ($p = +\infty$, $n = 100$). Warmer colors indicate significant performance degradation. For example, “red” means the most significant performance degradation while “blue” means the opposite. Results show that different neural networks exhibit diverse characteristics. Particularly, lower layers in ResNet-34 are more robust to parameter corruption while Transformer decoder shows the opposite trend.

A.4.4 MLP

We implement a MLP-based parser following [5] on a transition-based dependency parsing dataset provided by the English Penn TreeBank (PTB)[22]. We follow the standard splits of the dataset and adopt Unlabeled Attachment Score (UAS) as the evaluation metric. The hidden size is set to 512 and the batch size is 1,024. We use the Adam optimizer with an initial learning rate of 0.001. We evaluate the model on the development set every epoch and find the best checkpoint to evaluate the test results. The dropout rate is 0.2.

A.5 Supplement Experimental Results

In this section, we report supplement experimental results of our proposed parameter corruption approach to analyze and visualize the weak points of selected deep neural networks, which illustrates the divergent vulnerability of different components within a neural network.

A.5.1 Vulnerability in Terms of Parameter Positions

In our paper, we visualize the influence of parameter positions on the vulnerability of deep neural networks by applying the gradient-based gradient-based corruption consecutively to layers in ResNet-34 and Transformer. Several observations can be drawn from our paper: 1) Lower layers in ResNet-34 are less robust to parameter corruption and are prone to cause overall damage; 2) Upper layers in Transformer decoder are less robust to parameter corruption while the parameter corruption exhibits inconspicuous trend for Transformer Encoder.

In this section, we report some experimental results in Figure 6, Table 4 and Table 5 as the supplement experimental results for our work.

A.5.2 Choice of Hyper-parameters in Adversarial Training

For CIFAR-10 dataset, we choose $\epsilon \in \{0.05, 0.1, 0.2, 0.5, 1\}$, and for PTB-Parsing dataset, we choose $\lambda \in \{0.001, 0.002, 0.005, 0.01, 0.02\}$. The results are shown in Table 6. In our paper, we choose the hyper-parameters with best performance. Therefore, for CIFAR-10, $\epsilon = 0.5$, and for PTB-Parsing, $\lambda = 0.01$.

A.5.3 Detailed Visualization of the Vulnerability of Different Components in ResNet-34

In our paper, ResNet-34 is roughly divided into four layers. In this section, we report detailed visualization of the vulnerability of different components in ResNet-34 as shown in Figure 7. We can see that 1) Lower layers in ResNet-34 are more robust to parameter corruption; 2) Batch normalization in ResNet-34 is usually less robust to parameter corruption compared to its neighborhood components.

Table 4: Results of corrupting different layers ($p = 2, n = 100$) of ResNet-34 on ImageNet and CIFAR-10. \star denotes original performance scores without parameter corruption and scores close to the original score (difference less than 0.1).

Dataset		layer1	layer2	layer3	layer4
CIFAR-10	w/o Corruption			94.3 \star	
	$\epsilon = 10$	\star	\star	\star	\star
	$\epsilon = 20$	93.6	\star	87.6	\star
	$\epsilon = 50$	62.2	29.6	31.9	\star
	$\epsilon = 100$	13.5	13.2	11.8	92.5
	$\epsilon = 200$	10.0	10.1	10.3	71.4
	$\epsilon = 500$	10.0	10.9	9.8	30.7
ImageNet	w/o Corruption			72.5 \star	
	$\epsilon = 0.1$	72.2	\star	72.2	\star
	$\epsilon = 0.2$	71.7	72.1	71.7	\star
	$\epsilon = 0.5$	71.0	70.5	69.9	71.3
	$\epsilon = 1$	66.5	68.5	67.9	69.3
	$\epsilon = 2$	51.6	56.9	63.0	64.2
	$\epsilon = 5$	2.5	1.4	1.4	27.2
	$\epsilon = 10$	0.1	0.1	0.1	0.1

Table 5: Results of corrupting different layers ($n = 100, L_2$ -norm) of Transformer on De-En. \star denotes original performance scores without parameter attack and scores close to the original score (difference less than 0.1).

	layer1	layer2	layer3	layer4	layer5	layer6	
w/o Corruption			35.33 \star				
Encoder	$\epsilon = 0.1$	\star	\star	\star	\star	\star	
	$\epsilon = 0.2$	\star	\star	\star	\star	34.88	
	$\epsilon = 0.5$	\star	\star	29.89	35.06	\star	
	$\epsilon = 1$	\star	\star	9.68	33.54	35.04	
	$\epsilon = 2$	\star	27.23	0.53	2.79	32.85	
	$\epsilon = 5$	33.21	0.44	0.07	0.16	0.05	
	$\epsilon = 10$	5.8	0	0.05	0.11	0.55	
	$\epsilon = 20$	0.24	0	0.08	0.17	0.32	
Decoder	$\epsilon = 50$	0.04	0	0.11	0.17	0.33	
	$\epsilon = 0.1$	\star	\star	\star	\star	35.01	
	$\epsilon = 0.2$	\star	\star	\star	\star	34.40	
	$\epsilon = 0.5$	35.17	34.97	\star	35.21	35.07	
	$\epsilon = 1$	34.99	34.71	35.17	34.53	34.37	
	$\epsilon = 2$	33.86	33.08	32.09	31.00	32.00	
	$\epsilon = 5$	7.96	0.11	0.86	1.72	3.18	
						0.02	

Table 6: Results of different hyper-parameters in adversarial training.

CIFAR-10		PTB-Parsing	
ϵ	Δ Acc \uparrow	λ	Δ UAS \uparrow
0.05	+1.5	0.001	-0.2
0.1	+1.8	0.002	+0.1
0.2	+1.9	0.005	+0.3
0.5	+1.9	0.01	+0.6
1	+1.0	0.02	-0.1

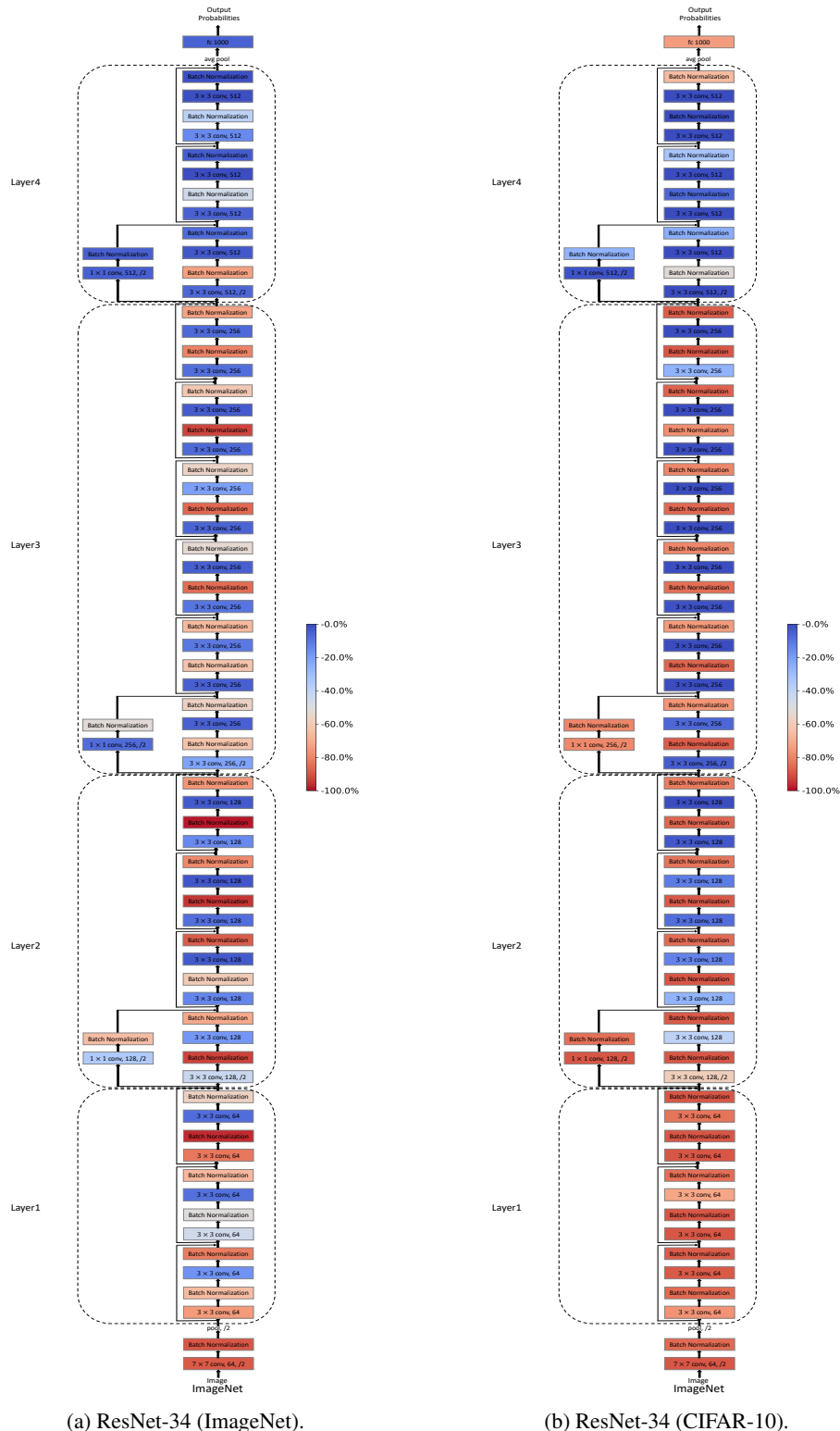


Figure 7: Detailed visualization of the vulnerability of different components in ResNet-34 and Transformer ($p = +\infty, n = 100$). ϵ is set to 0.5 for ResNet-34 (ImageNet) and 5 for ResNet-34 (CIFAR-10). Warmer colors indicate significant performance degradation. We can see that 1) Lower layers in ResNet-34 are more robust to parameter corruption; 2) Batch normalization in ResNet-34 are usually less robust to parameter corruption compared to its neighborhood components.